Full length article

Metal ablation study with a 10 picosecond laser under low and median fluence

Jian Cheng [a], Jiali Cao [a], Yi Huang [a], Stuart Edwardson [b], Walter Perrie [b], Geoff Dearden [b], Dun Liu [a]

[a] School of Mechanical Engineering, Hubei University of Technology, Wuhan 430068, China

[b] Laser Group, Department of Engineering, University of Liverpool, Brodie Building, Liverpool L69 3GQ, UK

ARTICLE INFO

Keywords
Picosecond laser processing
Metals and alloys
Modeling of laser ablation

ABSTRACT

Single shot 10ps laser ablation on aluminium and gold at a wavelength of 1064nm under low and median laser fluence was studied theoretically and experimentally. Simulations have been performed by using an optimized two temperature model. It is revealed that electron-phonon coupling ability of the target metal affected both the ablation depth and target metal's morphology. Under low fluence, melting could well be the relevant ablation mechanism. With laser fluence rising, vaporization or phase explosion happens thereafter, depending on mater-ial's electron-phonon coupling ability.

1. Introduction

Micro machining materials with ultrafast lasers – a technology first introduced in the early 1990s – is now widely studied and used routinely in many research areas, for instance thin film deposition, micro and nano hole drilling, writing waveguide, nano particles fabrication and ITO film scribing and patterning [1–6]. Photon-electron-phonon energy coupling considered, the negative effects associated with heat transfer could be minimized by using shorter laser pulse, say, from several tens of picosecond laser pulse down to several hundreds even tens of fem-tosecond laser pulse. Meanwhile, to keep the heat affected zone smaller than the optical skin depth, the input fluence is required to be kept in a low regime, just a few times above the ablation threshold (usually<1J/ cm_2), corresponding to laser pulse energy of the μJ level. Consequently, for most of the femtosecond high gain regenerative amplifier systems running at repetition rate of several kHz, mJ level output pulse energy have to be attenuated severely, thus wasting most of the throughput. While Chirped Pulse Amplification (CPA) leads to shorter pulse duration (which is definitely a huge advantage of femtosecond laser system), it considerably increases the complexity and cost of the machining oper-ation. Beam quality (M_2) becomes worse and not easy to control due to nonlinear interaction between the radiation and the atmospheric gas [7], which inversely affect the micro machining precision. All these is-sues need to be tackled before large scale industrial transfer becomes to reality.

Compared with femtosecond laser, picosecond laser has a longer pulse length of tens to hundreds times. This drawback may cause some thermal effect as for machining quality especially for metallic materials. However, its compactness, economy, good beam quality (usu-ally M_2 <1.15) and high repetition rate (up to MHz) raise more and more interests to industry. Previous study has demonstrated that two ab-lation regimes still exist for 10 picosecond pulse duration as with fem-tosecond pulse duration for metals with widely varying electron phonon coupling times [8]. By comparing experimental and modeling results, it is suggested under high fluence (>several J/cm_2), critical point phase separation (CPPS) may well be the ablation mechanism for 10ps laser metal ablation [9]. In this paper, a further study of this 10 picosec-ond laser metal ablation under low and median fluence has been carried out. Experimentally, ablation rate obtained by averaging hole depth of multi pulses drilling and morphology pictures achieved by single pulse drilling have been investigated quantitively and qualitatively, respec-tively. The classic one-dimensional, two-temperature model (TTM) has been improved to explore the ablation mechanism under this fluence regime. The electron thermal conductivity has also been investigated in this work.

2. Experimental

The laser and experimental set-up have been implemented as in Fig. 1. Simply to say, the output laser beam from a 10 picosecond laser system with the wavelength of 1064nm (HighQ IC-1500 Nd:VAN REG AMP) traversed a 3× beam expander and then directed to a scanning galvo (Nutfield, focal length:100mm). The laser beam pro-file can seriously affect the micromachining quality. In this study, a Spiricon beam profiler (Model LBA-300/400/500PC) was used to in-vestigate the laser beam profile. The measured raw beam diameter is 6.7mm with a nearly symmetry Gaussian shape as seen in Fig. 2. The measured focused spot size (1/e_2) was 22±0.2μm, almost dif

E-mail address: dun.liu@hbut.edu.cn (D. Liu)

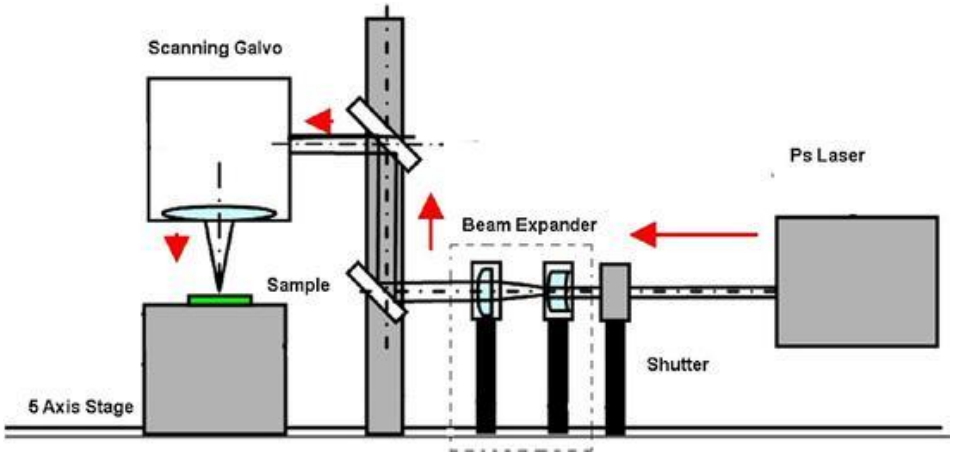

Fig. 1. Schematic illustration of the experimental set-up for picosecond laser ablation study. The laser beam went along the path as the red arrows showed and then finally was focused at the metal sample surface. The laser system, shutter, scanning galvo and stage were all controlled by one computer synchronously. (For interpretation of the references to colour in this figure legend, the reader is referred to the web version of this article.)

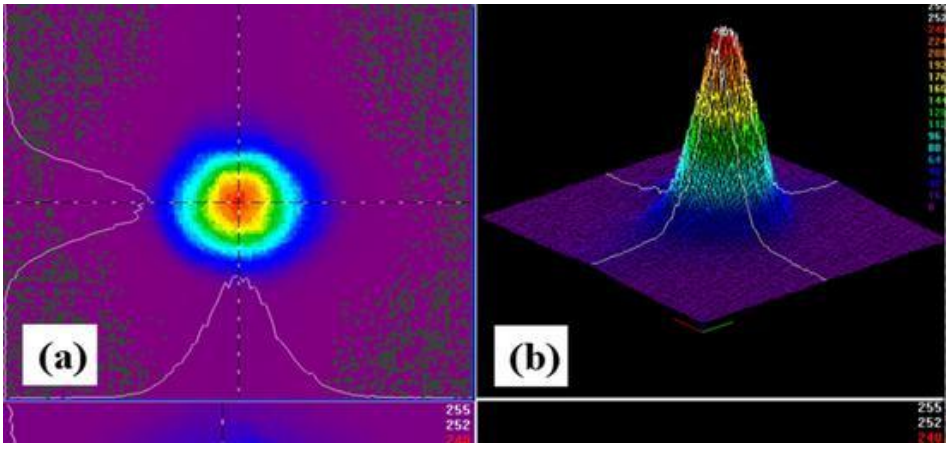

Fig. 2. (a) 2D and (b) 3D beam profiles of the 10 picosecond laser raw beam captured with a Spiricon beam profiler (Model LBA-300/400/500PC). The measured raw beam diameter is 6.7mm with a nearly symmetry Gaussian shape.

fraction limited. Samples were mounted on a 5-axis Aerotech stage which has a resolution down to 0.5 μm. The whole set-up was programmed, synchronized and controlled by a computer. The laser fluence could be continuously tuned with a half-wave plate. In this experiment, the pulse energy was varied in the range of 0.03–6 μJ, corresponding to a peak fluence range of 0.01–3J/cm^2.

Due to their different electron-phonon coupling performance, Al and Au were selected to do comparison study for this 10ps laser. Al has a free-electron-like structure while Au has a high electron density of state, associated with the d bands located ~2–3eV below the Fermi level. Samples of pure Al (99%) were polished and ground to an average surface roughness of 20nm; the gold sample (99.9%) was a gold layer (thickness: 500–600nm) with almost the similar surface roughness, which was coated on a copper mirror. Since under low laser fluence, ablation depth may become difficult to measure accurately from single pulse hole drilling, ablation rate were obtained by averaging holes' depth of multi pulses drilling. Meanwhile, morphology of sin-gle pulse drilling was observed without the influence of laser abla-tion plasma and incubation effects which could be achieved by set-ting long enough intervals between two consecutive pulses and hence simplifying theoretical modeling. Before and after laser ablation, the tested samples were processed in methanol by way of ultrasonic clean-ing to remove possible contamination and the ablated debris. Abla-tion depths were determined by using a WYKO NT1100 optical surface profiling system. Morphology of the ablated area was also captured with this instrument.

3. Computational model

Ultrashort pulse laser ablation of a metal target involves a cascade of processes: photon-electron energy coupling, energy transfer between the conduction band electrons and electron-lattice energy transfer until thermal equilibrium arrived. Since the heat capacity of degenerate elec-tron gas is small, the electron temperature follows, practically with al-most no delay, the shape of the laser pulse for the course of photon-elec-tron coupling [10]. Heat transfer between conduction electrons happens in several tens of fs to ps level which is related to laser pulse length. Heating of the lattice proceeds rather slowly in the range of several to more than 100ps, due to the great difference between electron and ion mass and heat capacity. To describe the energy transfer processes above, a two temperature model (TTM) was derived by Anisimov and Qiu from the classic Fourier law and the Boltzmann transport equation for elec-trons, respectively [11,12]:

$$C_e(T_e)\frac{\partial T_e}{\partial t} = \frac{\partial}{\partial z}\left(K_e\frac{\partial}{\partial z}T_e\right) - g(T_e - T_l) + S(z,t) \quad (1)$$

$$C_l(T_l)\frac{\partial T_l}{\partial t} = g(T_e - T_l) \quad (2)$$

C_e and C_l are the electronic and lattice heat capacities, respectively. K_e is the electron thermal conductivity, g is the electron-phonon coupling constant and the source term $S(z,t)$ is the absorbed laser energy density per unit time). The diffusive term can be neglected in the second equation due to a small part of energy it possesses. This model has been widely used and adapted in the investigation of ultrashort laser pulse ablation phenomenon in literature by numerous researchers (e.g., Refs. [13–16]).

Just as Lin et al has argued [17], a key issue in the application of the models above for quantitative description of the energy redistribution in the irradiated target is the choice of adequate temperature dependent thermophysical properties of the target material, say, the electron-phonon coupling constant, g, the electron heat capacity, C_e, and the electron therrmal conductivity, K_e. For example, Wang et al measured the electron-phonon coupling constant, g, at K_bT_e =1eV can increase to ~6 times of that value at room temperature with K_b being the Boltz-mann constant [18].

In this study, tabulated data of the electron-phonon coupling constant, g, and the electron heat capacity, C_e, are adopted which have taken the electron temperature dependence into account [19]. Figs. 3 and 4 indicated the electron temperature dependence of C_e and g for Al and Au, respectively.

As for the electron thermal conductivity, K_e, four equations have been mentioned to calculate its value [16,24,25]:

$$K_{e0} = K_0 \tag{3}$$

$$K_{e1} = K_0 \frac{T}{T_l} \tag{4}$$

$$K_{e2} = \frac{1}{3} V_F^2 \frac{C_e}{AT_e^2 + BT_l} \tag{5}$$

$$K_{e3} = C\vartheta_e \frac{(\vartheta_e^2 + 0.16)^{5/4}(\vartheta_e^2 + 0.44)}{(\vartheta_e^2 + 0.092)^{1/2}(\vartheta_e^2 + b\vartheta_l)} \tag{6}$$

K_0 is the electron thermal conductivity at electron-phonon thermal equilibrium. V_F is the mean velocity of electrons. At low electron temperatures, V_F is approximated as the Fermi velocity. A, B and C are material dependent constants. $\vartheta_e = T_e/T_F$ and $\vartheta_l = T_l/T_F$ with T_F being the Fermi temperature. Usually, Eqs. (4) or (5) is used to describe elec-tron thermal conductivity for low electron temperature and (6) will be more accurate when electron temperature arrives near to Fermi temper-ature [26]. Moreover, Eq. (4) is a simplified result of Eq. (5) with elec-tron-electron scattering effect neglected and is commonly used in calcu-lations. Comparison of the difference of these equations has been studied in several literatures [25,27,28]. However, all the results were based on the assumption of T_l =300K or electron-phonon thermal equilibrium acquired. In this study, similar work has been done but with a real time electron, phonon temperature changing process supposed to be irradi-ated with a 10ps laser pulse. In Fig. 5, a comparison of electron ther-mal conductivity for the metals investigated in this work, Al and Au, has been shown. For Au, predictions between Eqs. (4) and (5) showed not much difference, but a huge deviation can be seen for the prediction of Eq. (6). For Al, an obvious onset of deviation between the predictions of Eqs. (4) and (5) occurred, which indicated that ignoring the effect of electron scattering may cause a higher thermal conductivity. Since, in this paper the laser fluence used is in a low or moderate regime, electron temperatures for both metals are lower than Fermi temperature, Eq. (5) has been used in modelling work.

As for the source term, a Gaussian temporal profile is used to describe the laser energy deposition:

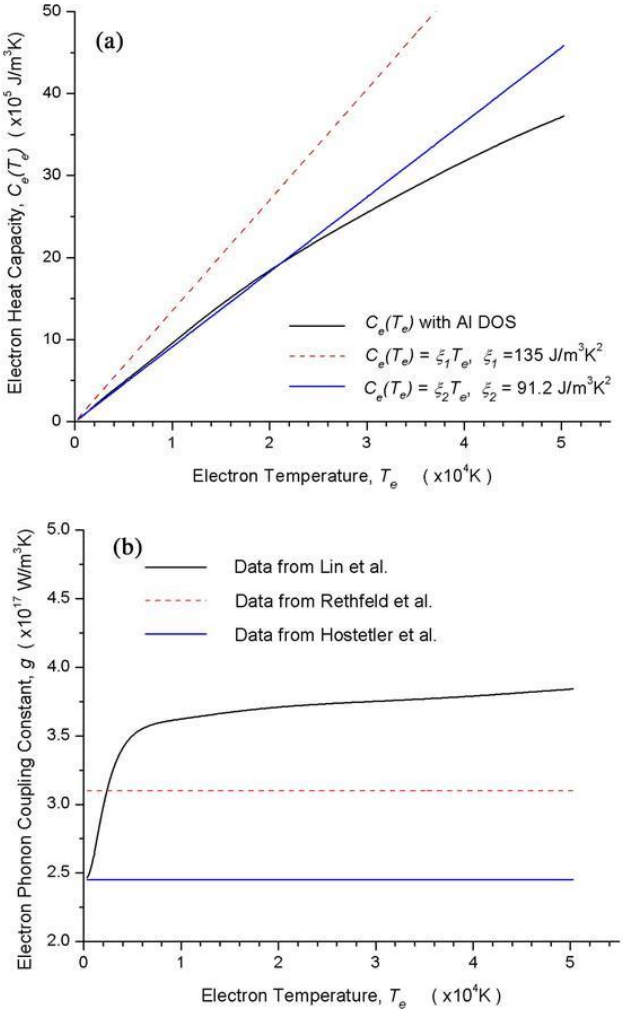

Fig. 3. (a) The electron heat capacity dependence on electron temperature for Al: red dashed line presents the experimental data from Ref. [20], blue line presents the theoreti-cal values calculated within the free electron gas model while black line presents the data calculated with electron density of state (DOS) by Lin et al. [19]. (b) The electron-phonon coupling constant dependence on electron temperature for Al: red dashed line presents the data from Ref. [21], blue line presents the data from Ref. [22] while black line presents the data calculated by Lin et al. [19]. (For interpretation of the references to colour in this figure legend, the reader is referred to the web version of this article.)

$$S(z,t) = J_0(1-R)d^{-1}\exp(-z/d)\exp\left(-4\ln 2\left(t-t_0\right)^2/\tau_p^2\right) \tag{7}$$

where I_0 is the peak intensity, R is the reflectivity, d is the skin depth, τ_p is the pulse duration (FWHM) and t_0 is time of the pulse centre. t_0 =12.8ps is adopted, corresponding to 3 times of the standard devia-tion of the Gaussian profile so that 99% of the pulse energy can be in-cluded.equation:I_0 can be related to the peak laser fluence with the following

$$F_{peak} = \sqrt{\pi/(4\ln 2)}\tau_p I_0 \tag{8}$$

This laser source was executed only on the electron system since electrons obtained most of the laser energy. No laser energy was assigned to the lattice system. The lattice system can only get energy from electron phonon coupling because of their huge temperature difference. Other data used in this model have been listed in Table 1.

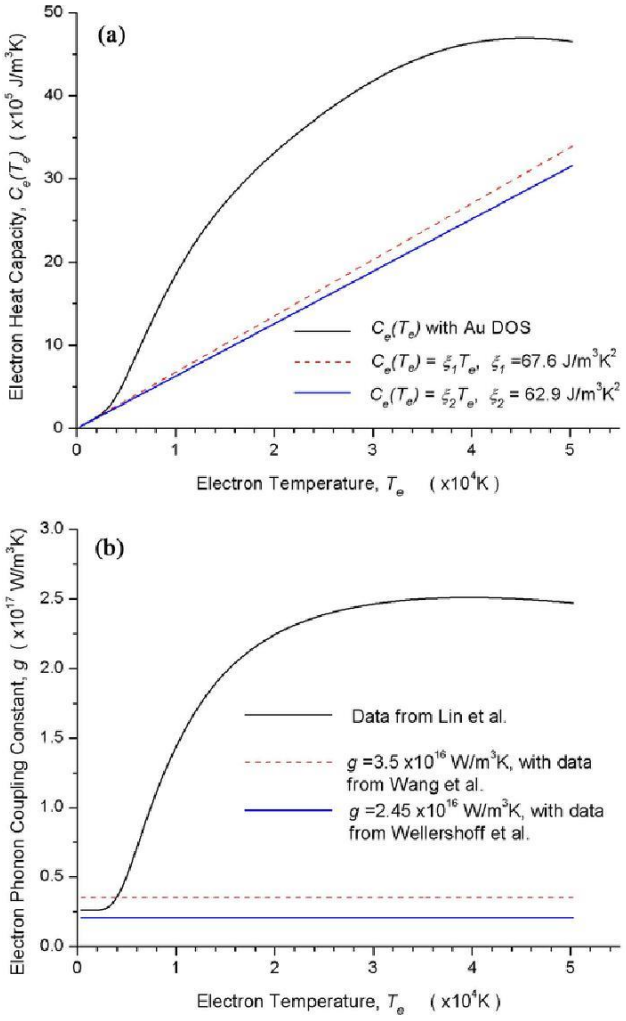

Fig. 4. (a) The electron heat capacity dependence on electron temperature for Au: red dashed line presents the experimental data from Ref. [20], blue line presents the theoreti-cal values calculated within the free electron gas model while black line presents the data calculated with electron density of state (DOS) by Lin et al. [19]. (b) The electron-phonon coupling constant dependence on electron temperature for Au: red dashed line presents the data from Ref. [18], blue line presents the data from Ref. [23] while black line pre-sents the data calculated by Lin et al. [19]. (For interpretation of the references to colour in this figure legend, the reader is referred to the web version of this article.)

4. Results and discussion

4.1. Ablation threshold prediction

To test the ablation threshold is a very important work for ultrafast laser ablation study. Below this value, ablation, i.e. measureable mater-ial removal, is impossible. It can be used to examine material properties for fundamental research; on the other hand, it helps to get the right laser fluence for high quality machining. However, it is very hard to get a direct threshold value just from the observation of the experimental re-sults, even with the help of high resolution SEM or TEM. Usually, an in-ferred threshold is obtained by extrapolating the trend line down to the coordinate axis by plotting D^2 vs fluence (logarithmic) [30]. By mod-eling, this inferred value can be verified and mechanism can be better understood.

When experimental and theoretical results are compared, one key issue is how to determine the optical reflectivity. Balling et al ob-served a significant reflectivity difference from the Fresnel reflectiv-ity and found it also changed during the ablation process due to the surface morphology changing and phase transition [25]. Following their suggestions, the reflectivity is used as a free fitting parameter in this work. The reflectivity of 0.5 and 0.93 for Al and Au are adopted, re-spectively. Moreover, the reflectivity of 0.5 for Al is very similar to the value of 0.58 in Ref. [25] and the reflectivity of 0.93 for Au fits 0.94 in Ref. [31] very well. With these assumptions, the abla-tion threshold of 0.015J/cm^2 and 0.872J/cm^2 for Al and Au are

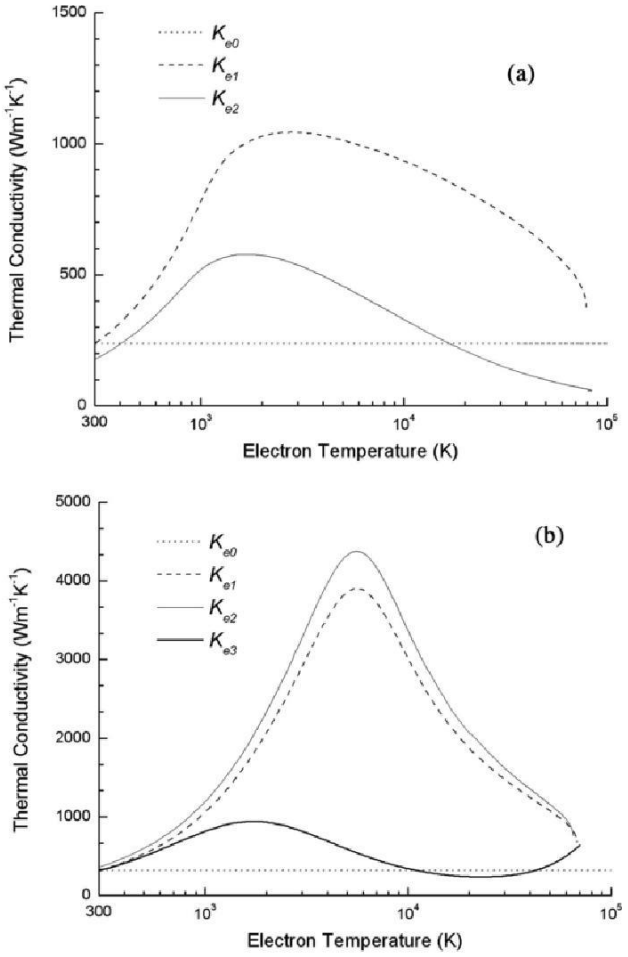

Fig. 5. A real time calculation of the electron thermal conductivity for Al (a) and Au (b) as a function of the electron temperature with different equations.

Table 1
Summary of the major material properties used in the model. Part of the data for Al are from Ref. [24]; part of data for Au are from Ref. [29].

	Al	Au
C_e (J/m^{3}K)	Ref. [19]	Ref. [19]
K_0 (W/m K)	235	318
V_F (×10^6 m/s)	2.03	1.40
d (nm)	17	14
Melting point (K)	933	1337
Evaporation pont (K)	2792	3080
Critical point (K)	5410	7400
A (×10^7/K^{2}s)	0.376	1.2
B (×10^{11}/Ks)	*3.9*	*1.23*
C (W/m K)	–	*353*
b	–	*0.16*

obtained respectively, corresponding to the experimental data of 0.01J/ cm_2 and 1.1J/cm_2 almost in the same order of magnitude.

4.2. Melting dominated regime

For fs laser ablation, ablation depth may be inferred with different mechanisms, for example, direct evaporation of target materials under low fluence [18] and critical point phase separation under high flu-ence [9,13]. With laser pulse duration increasing from fs to 10ps time regime, some changes may happen.

Figs. 6 and 7 illustrate the modeling temperature contour for melting, evaporation and critical point temperature along the direction inside the material with rising laser fluence for the studied metals. The experimental data of ablation depth have also been shown in the figures for comparison purpose. For this situation, only the

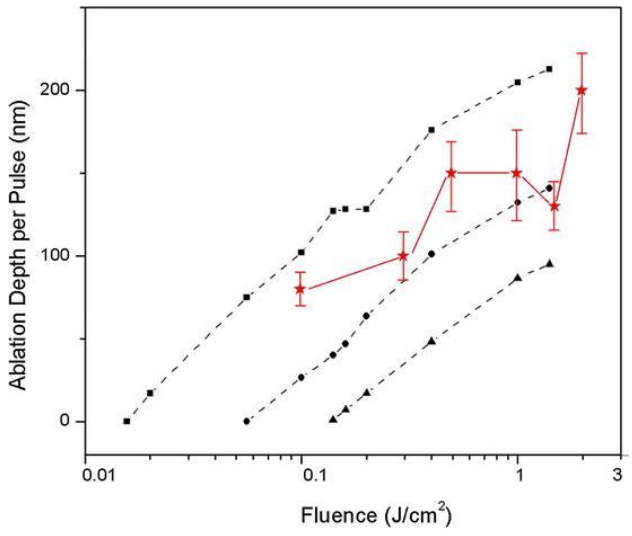

Fig. 6. A comparison of experimental data and simulation results for Al. The line signaled with black square presents the melting depth; The line signaled with black circle presents the evaporation depth; The line signaled with triangle presents the depth where critical point temperature arrived; The lines signaled with red star present the ablation depth from experiment. (For interpretation of the references to colour in this figure legend, the reader is referred to the web version of this article.)

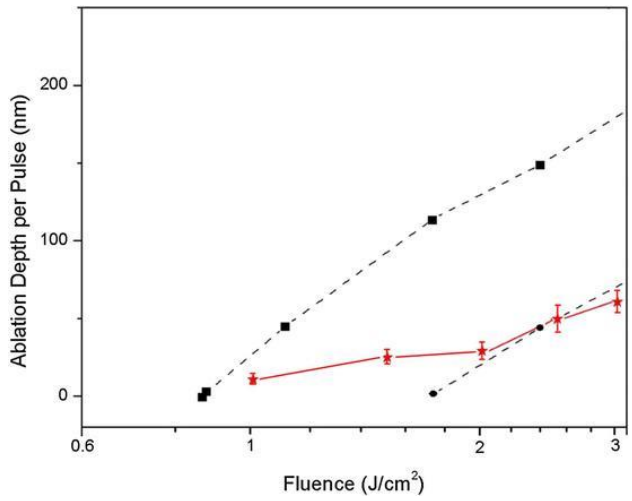

Fig. 7. A comparison of experimental data and simulation results for Au. The line signaled with black square presents the melting depth; The line signaled with black circle presents the evaporation depth; The lines signaled with red star present the ablation depth from experiment. (For interpretation of the references to colour in this figure legend, the reader is referred to the web version of this article.)

depth of the hole centre area was adopted as a valid value. Hence hole depths were estimated by averaging over five drilled holes at each flu-ence, indicated by the error bars in the corresponding figures. From these figures, it can be seen that the ablation depth is in the zone be-tween melting and evaporation, indicating almost no evaporation hap-pened and most of the ablation was caused by melting and the following liquid dynamic behaviour when laser fluences were below 1J/cm_2 for Al and 2J/cm_2 for Au, respectively (See Figs. 8 and 9 for sample surface morphology). Empirical results further show that the ablation rate of Al is much higher than that of Au. Due to a low melting point and strong electron-phonon coupling ability, a thicker melting layer and a follow-ing strong dynamical flowing performance can happen, enhance achieve high ablation rate. For Au, thermal energy can be transferred to a deeper depth and a larger volume thanks to its long electron-phonon coupling time, thus obtaining a gentle melting and less material removal. How-ever, melting always exists for this 10ps laser ablation under low flu-ence no matter what the electron-phonon coupling ability is.

4.3. Evaporation and phase explosion

With laser fluence further increasing and more energy being coupled into the lattice system, ablation rates rise for all the metals. The devi-ation of some points from the trend in Figs. 6 and 7 just revealed the transition status is unstable when melting jumps to a high level. Hence, their thermodynamic behaviours perform differently-large jump of ab-lation rate for Al can be expected with laser fluence >1.5J/cm_2 while no such obvious change for Au takes place.

Figs. 10 and 11 show the 2D and 3D morphology of the ablated area of the studied samples. Bubble-like structures and volcano-shaped morphology (Fig. 10) indicate that the melt liquid layer was overheated to a liquid-gas phase, described as phase explosion [13,32–34]. There-fore, phase explosion could well be the primary ablation mechanism for Al under this situation. In Fig. 11, the morphology of ablated Au sam-ple under a laser fluence of ~2.6J/cm_2 is presented. Different from Al, the ablated area of this Au sample looks very flat in the centre part. The ablation depth fits the evaporation depth of modeling very well, suggest-ing evaporation dominates in this laser fluence regime.

5. Conclusions

Single shot 10ps laser ablation on aluminium and gold at a wave-length of 1064nm under low and moderate laser fluence was studied theoretically and then compared with experimental results. Simulations indicated that electron-phonon coupling abilities of the target metals are heavily temperature-dependent. Based on this assumption, an optimized two temperature model was improved. From the model, it is revealed that electron-phonon coupling abilities affected both the ablation depth and target metals' morphology. Under low fluence, slight melting could well be the relevant ablation mechanism. With laser fluence increasing, vaporization or phase explosion happens thereafter for gold and alu-minium, depending on their own electron-phonon coupling abilities.

Acknowledgements

This work was partly supported by the National Natural Science Fund of China (Grant No. 51405141 and 51575164). The authors gratefully ac-knowledge their supports. Author Jian Cheng is particularly grateful to the Laser Group, University of Liverpool for its consistent support and help.

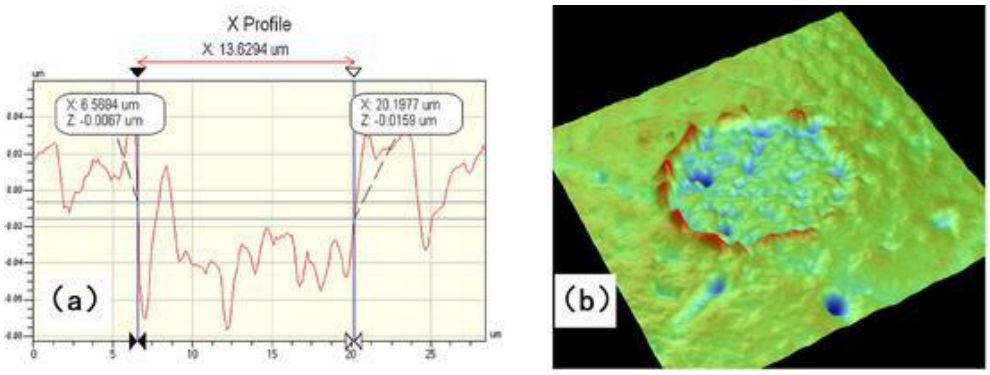

Fig. 8. Single pulse ablation images of Al sample under a laser fluence ~0.3J/cm^2. (a) 2D cross section profile and (b) 3D image captured with a WYKO NT1100 optical surface profiling system. The nearly flat irradiated area may indicate melting and thereafter re-solidification.

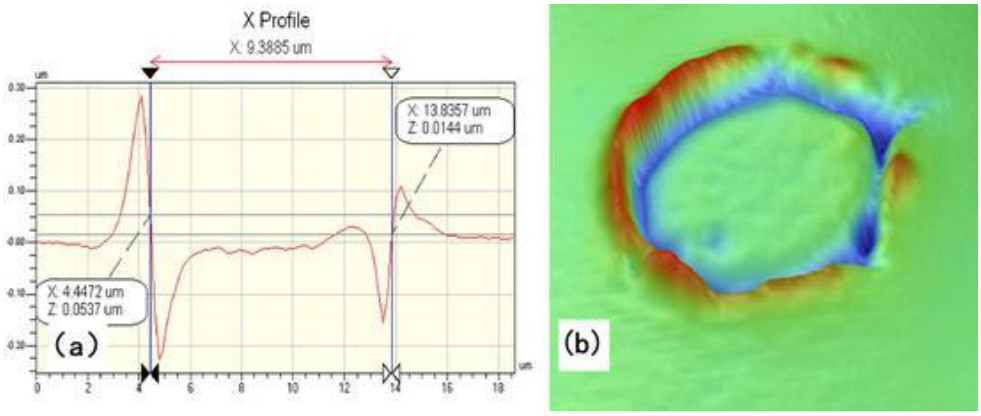

Fig. 9. Single pulse ablation images of Au sample under a laser fluence ~1.5J/cm^2. (a) 2D cross section profile and (b) 3D image captured with a WYKO NT1100 optical surface profiling system. The laser irradiated center area looks very flat, indicating a milder dynamic behavior when compared with Al.

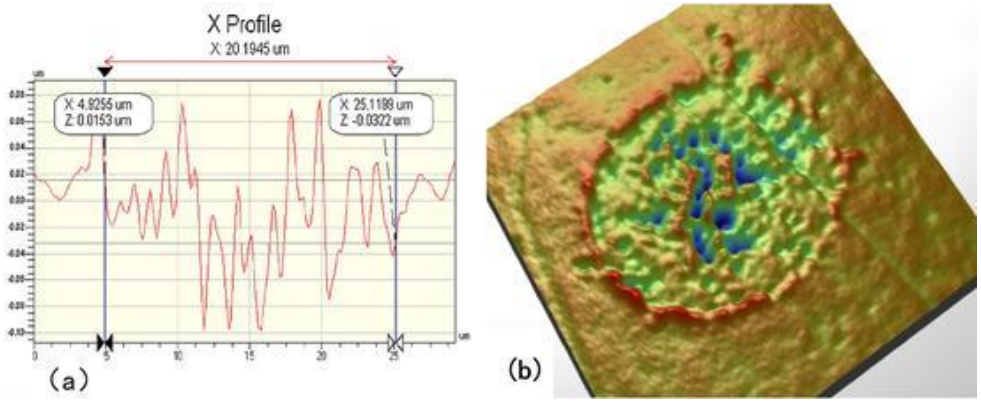

Fig. 10. Single pulse ablation images of Al sample under a laser fluence ~1.5J/cm^2. (a) 2D cross section profile and (b) 3D image captured with a WYKO NT1100 optical surface profiling system. The bubble-like structures show that Al undergoes phase explosion.

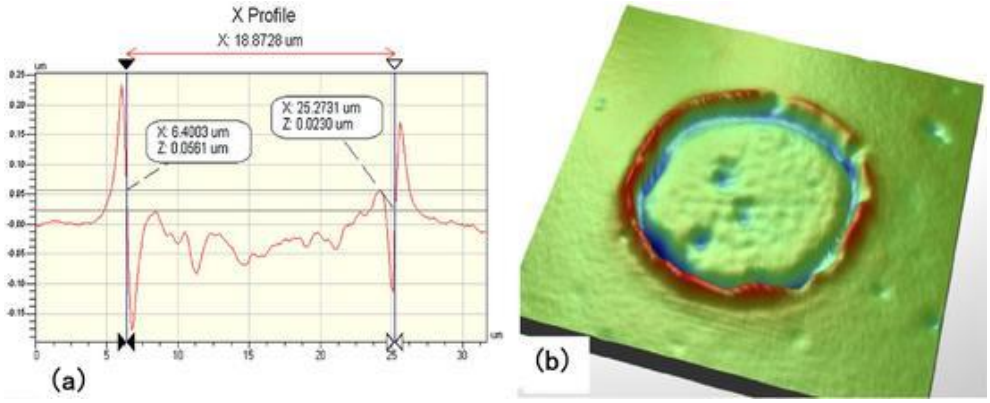

Fig. 11. Single pulse ablation images of Au sample under a laser fluence ~2.6J/cm^2. (a) 2D cross section profile and (b) 3D image captured with a WYKO NT1100 optical surface profiling system. The laser irradiated area still looked very flat, indicating a gentle evaporation process and no phase explosion happens.

References

[1] A.V. Rode, B. Luther-Davies, E.G. Gamaly, Ultrafast ablation with high-pulse-rate lasers. Part II: Experiments on laser deposition of amorphous carbon films, J. Appl. Phys. 85 (1999) 4213.

[2] B. Tan, S. Panchatsharam, K. Venkatakrishnan, High repetition rate femtosec-ond laser forming sub-10 μm diameter interconnection vias, J. Phys. D: Appl. Phys. 42 (2009) 065102.

[3] N. Farid, H. Chan, D. Milne, A. Brunton, G.M. O'Connor, Stress assisted selec-tive ablation of ITO thin film by picosecond laser, Appl. Surf. Sci. 427 (2018) 499.

[4] L. Bayer, M. Ehrhardt, P. Lorenz, S. Pisoni, S. Buecheler, A.N. Tiwari, K. Zim-mer, Morphology and topography of perovskite solar cell films ablated and scribed with short and ultrashort laser pulses, Appl. Surf. Sci. 416 (2017) 112.

[5] A. Talbi, A. Petit, A. Melhem, A. Stolz, C. Boulmer-Leborgne, G. Gautier, T. Def-forge, N. Semmar, Nanoparticles based laser-induced surface structures forma-tion on mesoporous silicon by picosecond laser beam interaction, Appl. Surf. Sci. 374 (2016) 31.

[6] J. Cheng, C.S. Liu, S. Shang, D. Liu, W. Perrie, G. Dearden, K. Watkins, A review of ultrafast laser materials micromachining, Opt. Laser Technol. 46 (2013) 88.

[7] R. Le Harzic, D. Breitling, M. Weikert, S. Sommer, C. FÖhl, S. Valette, C. Don-net, E. Audouard, F. Dausinger, Pulse width and energy influence on laser mi-cromachining of metals in a range of 100fs to 5ps, Appl. Surf. Sci. 249 (2005) 322.

[8] J. Cheng, W. Perrie, M. Sharp, S.P. Edwardson, N.G. Semaltianos, G. Dearden, K.G. Watkins, Single-pulse drilling study on Au, Al and Ti alloy by using a pi-cosecond laser, Appl. Phys. A 95 (2009) 739.

[9] J. Cheng, W. Perrie, B. Wu, S. Tao, S.P. Edwardson, G. Dearden, K.G. Watkins, Ablation mechanism study on metallic materials with a 10 ps laser under high fluence, Appl. Surf. Sci. 255 (2009) 8171.

[10] S.I. Anisimov, B. Rethfeld, On the theory of ultrashort laser pulse interaction with a metal, SPIE 3093 (1997) 192.

[11] S. Anisimov, B. Kapelovich, T. Perel'man, Electron emission from metal surfaces exposed to ultrashort laser pulses, Sov. Phys. JETP 39 (1974) 375.

[12] T.Q. Qiu, C.L. Tien, Heat transfer mechanisms during short-pulse laser heating of metals, J. Heat Transfer 115 (1993) 835.

[13] C. Cheng, X. Xu, Mechanisms of decomposition of metal during femtosecond laser ablation, Phys. Rev. B 72 (2005) 165415.

[14] J. Hohlfeld, S.-S. Wellershoff, J. Güdde, U. Conrad, V. Jähnke, E. Matthias, Elec-tron and lattice dynamics following optical excitation of metals, Chem. Phys. 251 (2000) 237.

[15] J.K. Chen, J.E. Beraun, Medelling of ultrashort laser ablation of gold films in vacuum, J. Opt. A: Pure Opt. 5 (2003) 168.

[16] J.K. Chen, J.E. Beraun, Numerical study of ultrashort laser pulse interactions with metal films, Numer. Heat Transfer: Part A 40 (2001) 1.

[17] Z. Lin, L.V. Zhigilei, V. Celli, Electron-phonon coupling and electron heat capac-ity of metals under conditions of strong electron-phonon nonequilibrium, Phys. Rev. B 77 (2008) 075133.

[18] X.Y. Wang, D.M. Riffe, Y.-S. Lee, M.C. Downer, Time-resolved electron-tempera-ture measurement in a highly excited gold target using femtosecond thermionic emission, Phys. Rev. B 50 (1994) 8016.

[19] Z. Lin, L. Zhigilei, <http://www.faculty.virginia.edu/CompMat/electron-phonon-coupling/>.

[20] D.E. Gray (Ed.), American Institute of Physics Handbook, McGraw-Hill, New York, 1972.

[21] B. Rethfeld, A. Kaiser, M. Vicanek, G. Simon, Ultrafast dynamics of nonequilib-rium electrons in metals under femtosecond laser irradiation, Phys. Rev. B 65 (21) (2002) 214303.

[22] J.L. Hostetler, A.N. Smith, D.M. Czajkowsky, P.M. Norris, Measurement of the electron-phonon coupling factor dependence on film thickness and grain size in Au, Cr, and Al, Appl. Opt. 38 (16) (1999) 3614.

[23] S.-S. Wellershoff, J. Hohlfeld, J. Güdde, E. Matthias, The role of elec-tron–phonon coupling in femtosecond laser damage of metals, Appl. Phys. A 69 (1999) S99.

[24] B.H. Christensen, K. Vestentoft, P. Balling, Short-pulse ablation rates and the two-temperature model, Appl. Surf. Sci. 253 (2007) 6347.

[25] K. Vestentpft, P. Balling, Formation of an extended nanostructured metal sur-face by ultra-short laser pulses: single-pulse ablation in the high-fluence limit, Appl. Phys. A Mater. Sci. Process. 84 (2006) 207.

[26] B. Rethfeld, Dissertation, TU Braunschweig, 1999.

[27] D.S. Ivanov, L.V. Zhigilei, Combined atomistic-continuum modeling of short-pulse laser melting and disintegration of metal films, Phys. Rev. B 68 (6) (2003) 064114.

[28] V. Schmidt, W. Husinsky, G. Betz, Ultrashort laser ablation of metals: pump–probe experiments, the role of ballistic electrons and the two-tempera-ture model, Appl. Surf. Sci. 197–198 (2002) 145.

[29] V. Kostrykin, M. Niessen, J. Jandeleit, W. Schulz, E.-W. Kreutz, R. Poprawe, Pi-cosecond laser pulses induces heat and mass transfer, Proc. SPIE 3343 (1998) 971.

[30] S. Nolte, C. Momma, H. Jacobs, A. Tünnermann, B.N. Chichkov, B. Wellege-hausen, H. Welling, Ablation of metals by ultrashort laser pulses, J. Opt. Soc. Am. B 14 (1997) 2716.

[31] P.P. Pronko, S.K. Dutta, D. Du, R.K. Singh, Thermophysical effects in laser pro-cessing of materials with picosecond and femtosecond pulses, J. Appl. Phys. 78 (10) (1995) 6233.

[32] D. Perez, L.J. Lewis, Molecular-dynamics study of ablation of solids under fem-tosecond laser pulses, Phys. Rev. B 67 (18) (2003) 184102.

[33] P. Lorazo, L.J. Lewis, M. Meunier, Thermodynamic pathways to melting, abla-tion, and solidification in absorbing solids under pulsed laser irradiation, Phys. Rev. B 73 (13) (2006) 134108.

[34] S. Amoruso, R. Bruzzese, X. Wang, N.N. Nedialkov, P.A. Atanasov, Femtosecond laser ablation of nickel in vacuum, J. Phys. D Appl. Phys. 40 (2007) 331.